SPACE WEATHER, VOL. 6, S10001, doi:10.1029/2008SW000391, 2008

A statistical comparison of commonly used external magnetic field models

J. P. McCollough,[1] J. L. Gannon,[2,3] D. N. Baker,[1] and M. Gehmeyr[1,2]

Received 29 January 2008; revised 11 June 2008; accepted 7 July 2008; published 3 October 2008.

[1] Accurate geomagnetic field models are crucial to the study of radiation belt phenomena. We quantitatively examine the accuracy of several external models widely in use via the Office National d'Etudes et de Recherche Aérospatiales-Département Environnement Spatial (ONERA-DESP) libraries. We study 2 years characterized by very different space weather conditions, 1996 and 2003. The year 1996, at solar minimum, exhibited many high-speed streams and a few corotating interaction regions but was generally quiet. In contrast, 2003 included the Halloween storm, one of the most intense geomagnetic storms on record caused by a coronal mass ejection. The performance of each model, as measured by prediction efficiency and skill score, is evaluated as a function of magnetospheric conditions (reflected by the geomagnetic index *Kp*) and magnetic local time (MLT). Not surprisingly, the newer models tend to perform better and interesting comparisons arise between the performances of the models during different periods of the solar cycle and across different *Kp* and MLT values. For $Kp < 4$, most models show similar performance, but for higher values, there are large differences between newer and older model performance. As a function of MLT, noticeable dips in the performance of older models are observed near dawn. These dips are suspected to be effects of field-aligned and partial ring currents that are not fully incorporated into the models, but their exact nature is unknown.

Citation: McCollough, J. P., J. L. Gannon, D. N. Baker, and M. Gehmeyr (2008), A statistical comparison of commonly used external magnetic field models, *Space Weather*, *6*, S10001, doi:10.1029/2008SW000391.

1. Introduction

[2] Accurately modeling Earth's magnetic field is important for a variety of reasons: to better understand the magnetosphere and its interactions with both the solar wind and thermosphere/ionosphere; to accurately model and better understand energetic particle dynamics in the radiation belts; and to better predict and understand geomagnetic storms. Studies comparing different magnetic field models have been done in the past [*Walker*, 1976; *Spence et al.*, 1987; *Peredo et al.*, 1993; *Stern*, 1994; *Reeves et al.*, 1996; *Thomsen et al.*, 1996; *Pulkkinen and Tsyganenko*, 1996], but did not include many models developed over the last decade. Recently, storm-specific studies have been done [*Huang et al.*, 2007; *Chen et al.*, 2007]. Our study complements these in that it is comprehensive and independent of particular storms. This study is concerned with overall performance at different disturbance levels for 2 very separate years situated at different phases of the solar cycle, one at solar minimum and one near solar maximum.

[3] The 2 years used in this study are 1996 and 2003. The year 1996 was characterized by a period of corotating interaction regions (CIRs), while 2003 included the interplanetary coronal mass ejection (CME) driven Halloween storm [*Baker et al.*, 2004]. By studying the performance of different external field models for these 2 years, marked by the two main physical mechanisms causing geomagnetic storms [*Kamide et al.*, 1998], we can determine how well the models perform in a variety of magnetospheric conditions.

1.1. *Kp* as a Measure of Magnetospheric Conditions

[4] In addition to overall performance, we look at how well the models perform for different levels of geomagnetic activity. We use *Kp* as a measure of magnetospheric activity. *Kp* is a planetary average of the K-index, a ground-based measurement which uses a quasi-logarithmic scale

[1]Laboratory for Atmospheric and Space Physics, University of Colorado, Boulder, Colorado, USA.
[2]Space Weather Prediction Center, National Oceanic and Atmospheric Administration, Boulder, Colorado, USA.
[3]Cooperative Institute for Research in Environmental Sciences, University of Colorado, Boulder, Colorado, USA.

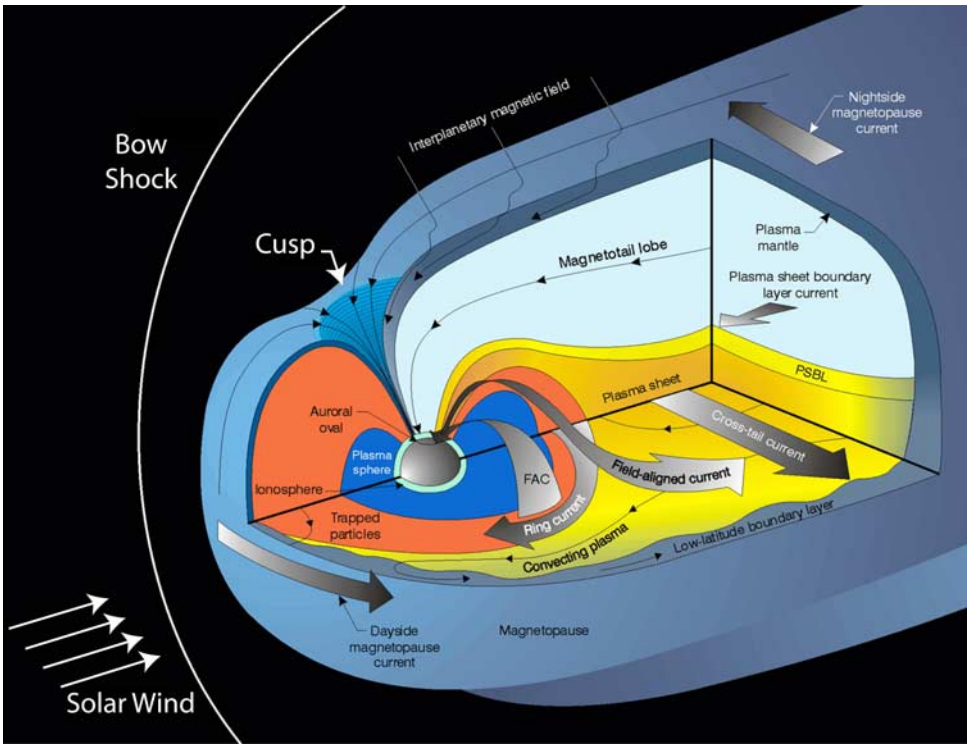

Figure 1. A schematic depiction of the major current systems and features of the magnetosphere. Note the omission of the partial ring current, which represents a transient part of the ring current that is not azimuthally symmetric. Adapted from a schematic diagram also used by *Baker et al.* [2005].

to characterize overall activity over a 3-h period using the observed peak variation of horizontal field components [*Tascione*, 1994; C. Balch, The K-index, 2007, available at http://www.swpc.noaa.gov/info/Kindex.html]. Unlike *Dst*, another commonly used index related to the strength of the ring current, *Kp* is not readily associated with a single current system (see Section 1.2). Thus, *Kp* provides a more generic indicator of geomagnetic disturbance.

1.2. Magnetosphere at Geosynchronous Orbit

[5] We focus our study on the geosynchronous orbit (6.6 R_E) for several reasons: first, the geomagnetic field in this region is highly dynamic; second, a vast amount of data is available for this region during the years of interest; third, geosynchronous orbit is densely populated by artificial satellites, and understanding the environment around them has significant economic and national interest. At geosynchronous orbit, the magnetic field is a superposition of that because of the Earth's internal tilted dipole and the external influence of magnetospheric current systems driven by the solar wind. The current systems exhibit dynamic changes, and the way these contributions are modeled is critical to the performance of a given model. The balance of solar wind dynamic pressure with magnetic pressure from Earth's magnetic field produces a day-night asymmetry with the field compressed on the dayside and stretched on the nightside. This pressure balance however is not fixed: solar wind speed and density, as well as the orientation of the embedded interplanetary magnetic field (IMF) are highly variable and this leads to disturbances and fluctuations in the field measured both at the Earth's surface and at geosynchronous orbit.

[6] The overall structure of the Earth's field can be understood through major current systems existing in different parts of the magnetosphere [see *Wolf*, 1995]. The primary magnetospheric current systems are the magnetopause current, the magnetotail current sheet, the ring and partial ring current, and Birkeland (field-aligned) currents (see Figure 1 [*Wolf*, 1995]). In addition to the day-night asymmetry that the magnetopause and magnetotail current sheets maintain, a significant dawn-dusk asymmetry in the external field exists because of the partial ring and Birkeland current systems. All of these current systems are influenced by the solar wind fluctuations noted above.

2. Models and Data

2.1. Models

[7] The models studied are empirical, but assume physical mechanisms embodied by the solar wind inputs and contributions from different current systems. Their performance indicates how accurate these assumptions and contributions are, and can indicate in which magnetospheric contexts they fail.

[8] We studied the Office National d'Etudes et de Recherche Aérospatiales-Département Environnement Spatial (ONERA-DESP) library V4.2 (D. Boscher et al., 2004–2008, available at http://wwwe.onecert.fr/craterre/support/user_guide.html) to compute field values from the external models supported by the library, with International Geomagnetic Reference Field (IGRF) as the internal field. The library provides the original implementations of many external models in one package. These models are (1) MF, *Fairfield and Mead* [1975]; (2) OPq, *Olson and Pfitzer* [1977] (quiet); (3) T87s, *Tsyganenko* [1987] (short); (4) T87ℓ, *Tsyganenko* [1987] (long); (5) OPd, *Pfitzer et al.* [1988] (dynamic); (6) T89, *Tsyganenko* [1989]; (7) T96, *Tsyganenko* [1995, 1996]; (8) OM, *Ostapenko and Maltsev* [1997]; (9) T02, *Tsyganenko* [2002a, 2002b]; and (10) TSK03, *Tsyganenko et al.* [2003]. The study was restricted to this library for consistency as well as simplicity. The library provides a uniform interface, as well as input bounds (see Section 4.4 for an important note regarding this) to ensure model usage only where appropriate. Brief descriptions of each model follow.

[9] MF uses *Kp* as its sole input and produces an external field using a second-order power series expansion in solar magnetic coordinates and dipole tilt

$$\Delta B_x = a_1 Z + a_2 XZ + T\left(a_3 + a_4 X + a_5 X^2 + a_6 Y^2 + a_7 Z^2\right), \quad (1)$$

$$\Delta B_y = b_1 YZ + T(b_2 Y + b_3 XY), \quad (2)$$

$$\Delta B_z = c_1 + c_2 X + c_3 X^2 + c_4 Y^2 + c_5 Z^2 + T(c_6 Z + c_7 XZ), \quad (3)$$

where (X, Y, Z) is the position and T is the dipole tilt angle. MF uses different sets of coefficients ($\{a_i\}$, $\{b_j\}$, $\{c_k\}$) for four different *Kp* ranges. It was one of the earliest data-based magnetospheric models.

[10] OPq has no inputs and is only meant to be used during quiet times. It uses a sixth-order power series expansion and exponential terms in position and tilt, and incorporates current contributions from the magnetopause, the current sheet, and the ring current.

[11] T87s and T87ℓ are variations on the same basic model, and use only *Kp*. They incoporate terms from the current sheet and the ring current, and differ in the number of internal parameters and range of validity: T87s includes 20 parameters and is applicable out to 30 R_E, and T87ℓ includes 26 parameters and is valid out to 70 R_E.

[12] OPd uses the solar wind density n, velocity v, and *Dst* as inputs to a power series expansion with magnetotail and ring current contributions. T89 uses *Kp*, and is an improvement on T87s/T87ℓ in that it incorporates terms from magnetotail warping (due to dipole tilt), and spatial variation of the current sheet. In addition, truncation factors are added to represent the finite extent of the current sheet.

[13] T96 uses *Dst*, the dynamic pressure $p = nv^2$ of the solar wind, and the y and z GSM components of the IMF. It includes terms from the magnetotail current sheet, ring current, magnetopause current, and, notably, terms for Birkeland (field-aligned) currents.

[14] OM uses *Kp*, *Dst*, p, and the z component of the IMF as inputs to a fourth-order power series expansion in position. It is not a current-based model: it has six terms that are azimuthally symmetric, six to account for day-night asymmetry, and five for dipole tilt.

[15] T02 and TSK03 use *Dst*, p, the y and z IMF components, and three parameters defined below: $G1$ (T02), $G2$ (T02 and TSK03), and $G3$ (TSK03). Both models account for contributions from the magnetotail current sheet, ring current, magnetopause current, Birkeland currents, and the partial ring current with field-aligned closure currents. These models update T96 in the methods used and provide for dawn-dusk asymmetry via the partial ring current.

[16] The G parameters are defined as follows (all components in GSM coordinates, and B refers to the IMF):

$$G1 = \left\langle v \frac{(B_\perp/40)^2}{(1 + B_\perp/40)} \sin^3(\theta/2) \right\rangle, \quad (4)$$

$$G2 = 0.005\langle vB_s \rangle, \quad (5)$$

$$G3 = \left\langle \frac{nvB_s}{2000} \right\rangle, \quad (6)$$

where $\langle\rangle$ denotes the average over the previous hour, and

$$B_\perp = \sqrt{B_y^2 + B_z^2} \quad (7)$$

$$B_s = \begin{cases} 0 & : \quad B_z \geq 0 \\ -B_z & : \quad B_z < 0 \end{cases}, \quad (8)$$

$$\theta = \begin{cases} \arctan\frac{|B_y|}{B_z} & : \quad B_z \geq 0 \\ 180.0^\circ - \arctan\frac{|B_y|}{B_z} & : \quad B_z < 0 \end{cases}, \quad (9)$$

are common solar wind-magnetosphere coupling parameters. There are two key differences between T02 and TSK03: the use of $G3$ instead of $G1$, and the data sources. Whereas T02 used data from 1984–1999, TSK03 used only data collected during major geomagnetic storms from 1996 to 2000 to generate its coefficients.

[17] Two other models are included in the ONERA libraries but are not examined in this study: *Alexeev et al.* [2000] and *Tsyganenko* [2005]. This is due to insurmountable usage complications in the former, and the storm-specific nature of the latter.

Table 1. Overall Results[a]

	1996						2003					
	GOES-8			GOES-9			GOES-10			GOES-12		
Model	PE	SS	CC	PE	SS	CC	PE	SS	CC	PE	SS	CC
Tsyganenko et al. [2003]	0.80	0.29	0.91	0.83	0.37	0.91	0.69	0.26	0.83	0.58	0.20	0.79
Tsyganenko [2002a, 2002b]	0.84	0.36	0.86	0.86	0.42	0.85	0.85	0.49	0.72	0.80	0.45	0.65
Ostapenko and Maltsev [1997]	0.82	0.32	0.91	0.73	0.21	0.87	0.32	−0.08	0.70	0.24	−0.08	0.72
Tsyganenko [1995, 1996]	0.67	0.09	0.86	0.74	0.22	0.90	0.70	0.28	0.81	0.68	0.30	0.73
Pfitzer et al. [1988]	0.73	0.18	0.92	0.80	0.32	0.95	0.58	0.15	0.97	0.30	−0.04	0.75
Olson Pfitzer [1977]	0.60	0.00	0.82	0.56	0.00	0.84	0.42	0.00	0.75	0.35	0.00	0.60
Tsyganenko [1989]	0.70	0.14	0.87	0.74	0.23	0.88	0.64	0.21	0.81	0.53	0.15	0.76
Tsyganenko [1987] long	0.17	−0.44	0.71	0.30	−0.26	0.76	0.40	−0.02	0.73	−0.04	−0.26	0.68
Tsyganenko [1987] short	0.67	0.10	0.86	0.67	0.13	0.87	0.57	0.14	0.77	0.35	−0.00	0.70
Fairfield and Mead [1975]	0.57	−0.04	0.84	0.58	0.02	0.87	0.51	0.08	0.79	0.08	−0.19	0.66

[a]PE, SS, and CC are prediction efficiency, skill score, and correlation coefficient, respectively. We used OPq as the reference model in calculating skill score.

2.2. Data

[18] The various magnetospheric input data used in the models are provided from the ACE and WIND satellites via the OMNI/OMNI2 data sets (N. Papitashvili, OMNIWeb, 2007, available at http://omniweb.gsfc.nasa.gov/). The parameters used depend on the model employed; in general, geomagnetic indices (*Kp*, *Dst*, etc.) are used as well as solar wind parameters (flow speed, dynamic pressure, density, IMF orientation, and derived coupling parameters).

[19] To assess the accuracy of the model output, GOES-8, GOES-9, GOES-10, and GOES-12 magnetic field observations (H. J. Singer, Coordinated Data Analysis Web, 2007, available at http://cdaweb.gsfc.nasa.gov/) were tabulated. In order to eliminate errors from position changes, the positions from the GOES data were used to determine the position at which to calculate the model field.

[20] The observed field values for GOES-8 and GOES-10 have known offsets [*Tsyganenko et al.*, 2003] of 7.22 nT and 1.04 nT, respectively, in the GSM z component, and these offsets were subtracted before the program wrote the output. A systematic study of GOES-9 and GOES-12 data has not been done, thus no offsets were assumed for these satellites.

3. Methodology

[21] Statistical methods [*Vassiliadis*, 2007], including skill score and prediction efficiency, are used to determine which models most closely follow observations from GOES satellite measurements for the calendar years 1996 and 2003. When calculating the accuracy of a model, one often uses the linear correlation coefficient

$$C_{\hat{x},x} = \frac{1}{N}\frac{1}{\sigma_{\hat{x}}\sigma_x}\sum_{i=1}^{N}(\hat{x}_i - \langle\hat{x}_i\rangle)(x_i - \langle x_i\rangle), \tag{10}$$

where $\hat{x}$ is the model value, x is the observed data, N is the size of the sample, and σ denotes standard deviation. In reality, this quantity is intended to compare two sets of different types of data, not two quantities that should have the same value (i.e., the mean values should be included in the metric). While linear correlation coefficient describes how well trends in one set of data are exhibited in another, it does not provide any gauge of how close the two are to the same value. Since the latter is what we have as our goal, we use prediction efficiency (PE), defined in terms of root-mean-square error [*Vassiliadis*, 2007]

$$\mathrm{PE} = 1 - \frac{e_{\mathrm{rms}}^2}{\sigma_x^2}, \tag{11}$$

$$e_{\mathrm{rms}} = \sqrt{\frac{1}{N}\sum_{i=1}^{N}(\hat{x}_i - x_i)^2}. \tag{12}$$

[22] The PE is a quantity that measures how much of the variation in the observed data can be explained by the model. Its values lie within $(-\infty, 1]$, with 1 indicating that the model is perfectly accurate, 0 indicating that the model is no better than a "model" that is the mean value of the data, and negative values show that the model is worse than the mean model.

[23] To go one step further, we can calculate the relative performance of one model versus another reference model via the skill score (SS)

$$\mathrm{SS} = 1 - \frac{e_{\mathrm{rms}}^2}{\left(e_{\mathrm{rms}}^{(\mathrm{ref})}\right)^2}, \tag{13}$$

where the difference from PE is that the denominator is now the rms error for the reference model. These quantities have been calculated for the years in question, as well as subsets of those years (discriminated by *Kp* and magnetic local time).

4. Results

4.1. Overall Performance

[24] Table 1 shows the overall performance of the models over the years 1996 and 2003. This analysis considers

Table 2. Quiet Results: $Kp \in [0, 3]$ Periods[a]

	1996						2003					
	GOES-8			GOES-9			GOES-10			GOES-12		
Model	PE	SS	CC	PE	SS	CC	PE	SS	CC	PE	SS	CC
Tsyganenko et al. [2003]	0.83	0.31	0.93	0.84	0.37	0.92	0.80	0.34	0.90	0.72	0.21	0.87
Tsyganenko [2002a, 2002b]	0.85	0.35	0.88	0.86	0.40	0.87	0.85	0.43	0.77	0.78	0.29	0.76
Ostapenko and Maltsev [1997]	0.87	0.39	0.94	0.74	0.18	0.88	0.51	−0.04	0.77	0.55	−0.01	0.84
Tsyganenko [1995, 1996]	0.70	0.09	0.88	0.74	0.18	0.91	0.70	0.19	0.88	0.67	0.13	0.85
Pfitzer et al. [1988]	0.76	0.18	0.94	0.80	0.28	0.96	0.64	0.11	1.11	0.38	−0.19	0.94
Olson and Pfitzer [1977]	0.64	0.00	0.85	0.61	0.00	0.85	0.55	0.00	0.82	0.56	0.00	0.76
Tsyganenko [1989]	0.74	0.14	0.89	0.75	0.20	0.89	0.73	0.22	0.86	0.66	0.12	0.84
Tsyganenko [1987] long	0.13	−0.56	0.71	0.23	−0.41	0.77	0.29	−0.25	0.75	−0.08	−0.57	0.73
Tsyganenko [1987] short	0.70	0.09	0.89	0.68	0.09	0.88	0.64	0.11	0.83	0.57	0.01	0.82
Fairfield and Mead [1975]	0.60	−0.05	0.87	0.58	−0.03	0.87	0.57	0.03	0.83	0.36	−0.21	0.80

[a]PE, SS, and CC are prediction efficiency, skill score, and correlation coefficient, respectively. We used OPq as the reference model in calculating skill score.

all data points within the valid input range, which varies between models (see Section 4.4). Two GOES satellites were in orbit for each of these years (GOES-8 and GOES-9 for 1996, and GOES-10 and GOES-8/12 for 2003), which provided four data sets. (For the year 2003, GOES-10 was operating as GOES-West. GOES-8 was GOES-East until March, when it was replaced by GOES-12.) Prediction efficiency, skill score, and correlation coefficient were tabulated for each model and satellite. For skill score, the reference model used was OPq, since it is a static baseline model.

[25] As can be seen, the newest models tended to perform best, although there are exceptions: OPd performed better in 1996 than T96, and performance was better in 1996 than 2003 overall. Notice that the relation between correlation coefficient and prediction efficiency is not as straightforward as some suggest. Also note that some older models perform worse than OPq.

[26] The performance of T87ℓ was very low, even relative to T87s. The cause of this is not known. However, as indicated by the correlation coefficient, T87ℓ captures the trends in the observed data as well as some other models. Thus, it seems to have a significant offset, and T8ℓ should not be used as is.

[27] A key point seen in Table 1 is that while some models are markedly better than others, no model is perfect, and the nature of a user's intention may dictate the choice of field model. This point is discussed further in Section 5.5.

4.2. Performance as a Function of *Kp*

[28] The dependence of prediction efficiency on *Kp* is examined in two ways: by looking at performance for quiet ($Kp \in [0, 3]$) and disturbed ($Kp \in [6, 9]$) periods; and by looking at performance for each of the 28 possible *Kp* values. The quiet performance is shown in Table 2. Not surprisingly, most models perform better during these periods than they do overall, and roughly the same relative to each other. Disturbed performance is shown in Table 3. Performance across all models is degraded, but the newer ones (with the exception of OM) seem to be more robust; that is, the models had less of a performance loss during more disturbed periods. "Robust" here is used in a relative sense. The quantity that it most closely corresponds to is the slope of the PE as a function of *Kp* (see Figures 2 and 3). The steeper the slope, the less robust a model is, relative to the other models studied.

[29] The relatively poor performance of TSK03 relative to T02 is most likely due to an input bias in sampling. T02 has limits on its inputs, while TSK03 accepts any value of magnetospheric input. This means that, particularly in disturbed periods, T02 will occasionally output a "bad data" flag (a feature of the ONERA implementation of the libraries that occurs whenever the input values to a given model

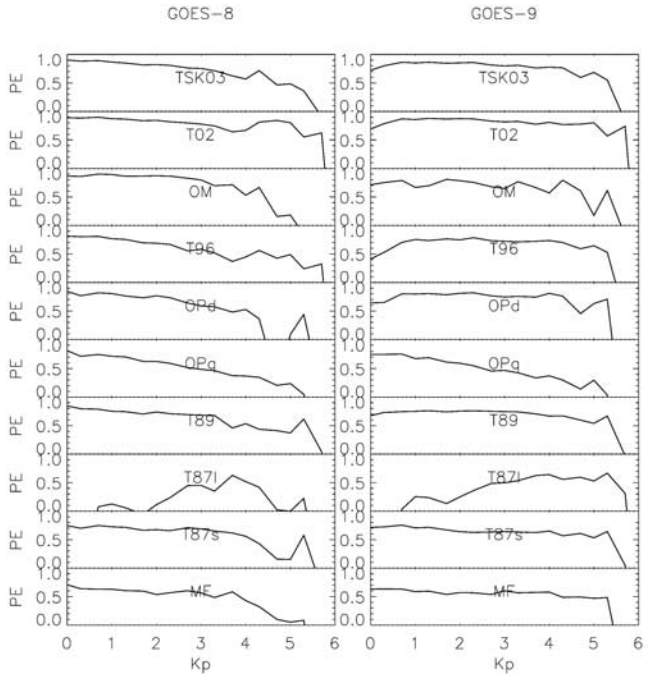

Figure 2. Prediction efficiency as a function of *Kp* for 1996. Beyond *Kp* = 6, the values go negative because of a lack of performance and a lack of data points for the highest values (8- and greater).

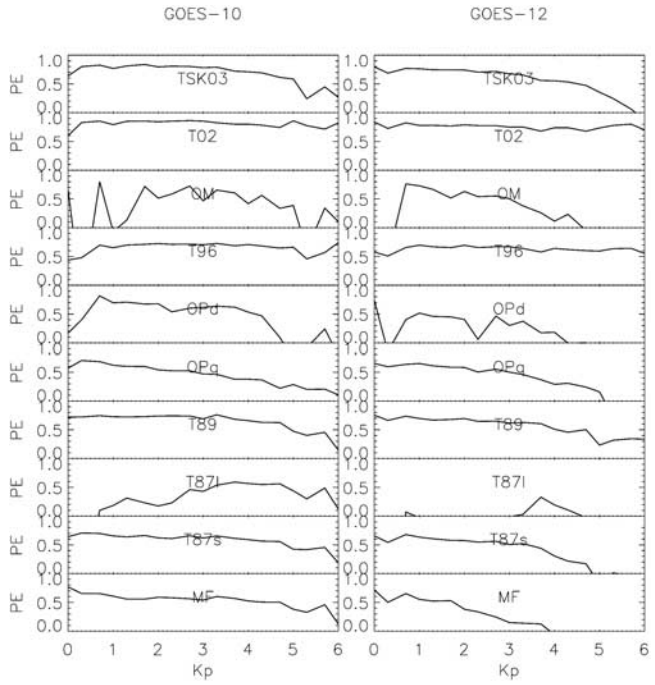

Figure 3. Prediction efficiency as a function of *Kp* for 2003. Beyond *Kp* = 6, the values go negative because of a lack of performance and a lack of data points for the highest values (8- and greater).

are outside the range which the model can handle), but TSK03 attempts to provide a field value anyway, as it has no bounds on its inputs. In addition, the slight advantage T02 has over TSK03 in general is probably due to the fact that TSK03 only uses storm data to train the model, whereas T02 used quiet and disturbed periods.

[30] For further detail, we examined prediction efficiency for each *Kp* value. Figures 2 and 3 show plots of these results. Beyond Kp = 6, prediction efficiencies often became negative because of lack of performance, and, particularly for *Kp* = 8- and greater, lack of data points.

[31] Most models showed a gradual downward trend from best performance near *Kp* = 0 to bad performance for disturbed periods. T02 and TSK03 appear to be most robust on the basis of these results.

4.3. Performance as a Function of Magnetic Local Time

[32] Prediction efficiencies were also examined for each hour in magnetic local time. Magnetic local time (MLT) is analogous to local time, but instead of using longitude to delineate ''time zones,'' magnetic longitude is used. MLT values run from 00:00 to 23:59, with 6:00 dawn, 12:00 noon, and 18:00 dusk.

[33] Figures 4 and 5 show the prediction efficiency profiles against MLT for 1996 and 2003, respectively. Note that the older models perform their worst on the dayside, while newer ones do their best on the dayside. Also note some models have a conspicuous dip near dawn. These profiles are very intriguing, and the bulk of the following discussion will be concerned with them.

4.4. Model Input Bias

[34] An important point should be noted when examining Tables 1–3; the models have different acceptable input ranges (see Table 4), which means that the collection of data points used varies from model to model. This is not significant for most models (most data points are similar), but T02 has a significant input bias to quiet conditions. The limits on inputs listed in Table 4 are found in the ONERA-DESP documentation (D. Boscher et al., 2004–2008, available at http://wwwe.onecert.fr/craterre/support/user_guide.html), and were ''determined through discussion with the model authors and statistics from the input parameter range used to define model fits,'' (S. Bourdarie, Input range in the T02 model, personal communication, 2008).

[35] The net effect of this input bias is to significantly enhance the performance of T02 relative to the other models. Table 4 shows how performance changes when the only data points used are those valid for T02. The marked increase in prediction efficiency of all models when significantly limiting the valid times to only those

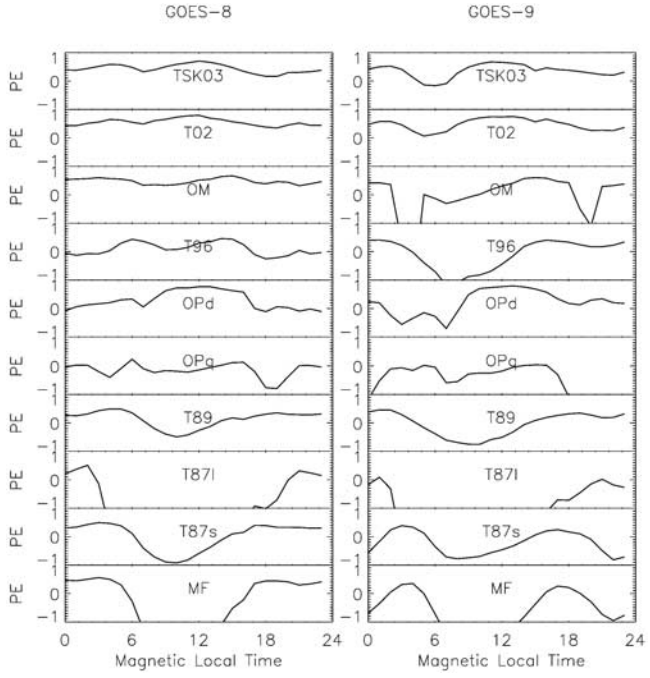

Figure 4. Prediction efficiency as a function of magnetic local time for 1996. Notice the three types of profiles discussed in section 5.

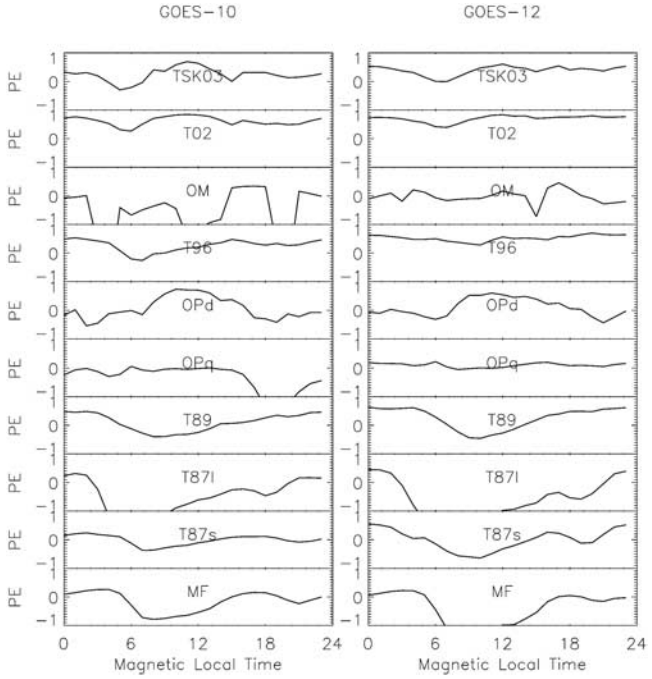

Figure 5. Prediction efficiency as a function of magnetic local time for 2003. Notice the three types of profiles discussed in section 5 and the differences from year 1996.

accepted by T02 highlights the difficulty of modeling the highly variable storm time field.

5. Discussion

[36] The above results suggest models can be broken down into three main classes: basic, symmetric, and asymmetric. The "symmetry" suggested in the labels is the dawn-dusk symmetry incorporated into, or excluded from, the models. That is, whether or not the models incorporate elements that can lead to a dawn-dusk asymmetry in the magnetic field.

5.1. Basic Models

[37] Basic models are distinguished in the data by strong, broad dayside dips in prediction efficiency (see Figures 4 and 5). There are four basic models: MF, TS87s, TS87ℓ, and T89. These are all models that attempt to provide gross pictures of the magnetosphere, generally during quiet times. Most notably, these models are the ones that do not use any solar wind input (either no inputs at all or only *Kp*). It is apparent that the dayside is not adequately modeled without including solar wind coupling parameters to some degree.

5.2. Symmetric Models

[38] Symmetric models (OPq, OPd, and OM) do not show the characteristic dayside dip of basic models, but have localized dips near dawn and dusk, with strong performance near magnetic noon. These models are those that do not incorporate the partial ring current or Birkeland currents, but do incorporate more detailed dynamics than basic models through either advanced modeling schemes (OPq) or coupling to the solar wind (OPd, OM). These models have stronger overall performance than basic models.

5.3. Asymmetric Models

[39] Tsyganenko's later models (T96, T02, and TSK03) were explicitly designed with dawn-dusk asymmetry in mind [*Tsyganenko and Stern*, 1996; *Tsyganenko*, 1995, 1996, 2002a, 2002b]. These models still have dawn and dusk dips (with the dawn dip noticeably larger in most cases), but they are much smoother than the symmetric model profiles. The incorporation of field-aligned currents and/or the partial ring current obviously improves performance compared to the other classes, but it seems there are still some unaccounted for residual effects.

5.4. Solar Activity in 1996 Versus 2003

[40] The characteristics of the classes described above depend upon solar activity. They are most clear cut at solar minimum (1996), but can still be seen in the declining phase near solar maximum (2003). While 1996 was

Table 3. Disturbed Results: $Kp \in [6, 9]$ Periods[a]

	1996						2003					
	GOES-8			GOES-9			GOES-10			GOES-12		
Model	PE	SS	CC	PE	SS	CC	PE	SS	CC	PE	SS	CC
Tsyganenko et al. [2003]	0.37	0.15	0.62	0.65	0.33	0.83	0.32	0.07	0.66	0.30	0.21	0.69
Tsyganenko [2002a, 2002b]	0.72	0.43	0.47	0.74	0.42	0.69	0.85	0.57	0.52	0.83	0.61	0.35
Ostapenko and Maltsev [1997]	−0.08	−0.12	0.58	0.39	0.11	0.69	−0.64	−0.44	0.47	−0.36	−0.10	0.57
Tsyganenko [1995, 1996]	0.41	0.17	0.71	0.62	0.29	0.74	0.68	0.36	0.61	0.73	0.51	0.53
Pfitzer et al. [1988]	0.06	−0.04	0.66	0.62	0.30	1.07	0.14	−0.04	0.49	−0.32	−0.08	0.15
Olson and Pfitzer [1977]	0.14	0.00	0.38	0.23	0.00	0.76	0.21	0.00	0.50	−0.12	0.00	0.21
Tsyganenko [1989]	0.41	0.17	0.65	0.53	0.22	0.77	0.31	0.07	0.61	0.21	0.16	0.54
Tsyganenko [1987] long	−0.07	−0.11	0.64	0.59	0.27	0.82	0.28	0.05	0.61	−0.41	−0.12	0.46
Tsyganenko [1987] short	0.21	0.04	0.64	0.59	0.27	0.79	0.32	0.08	0.59	−0.16	−0.01	0.46
Fairfield and Mead [1975]	−0.07	−0.11	0.52	0.48	0.18	0.83	0.27	0.04	0.59	−0.47	−0.14	0.38

[a]PE, SS, and CC are prediction efficiency, skill score, and correlation coefficient, respectively. We used OPq as the reference model in calculating skill score.

Table 4. Input Ranges and Prediction Efficiencies for Only the Valid T02 Data Points and for All Data Points Valid for the Given Model (From Table 1)[a]

Model	Input Ranges	PE (T02 Points)	PE (All Points)
Tsyganenko et al. [2003]	None	0.85164324	0.68731874
Tsyganenko [2002a, 2002b]	$-50 \le Dst \le 20$, $0.5 \le p \le 5$, $\lvert B_y\rvert \le 10$, $\lvert B_z\rvert \le 10$, $0 \le G1 \le 10$, $0 \le G2 \le 10$	0.84759047	0.84759047
Ostapenko and Maltsev [1997]	None	0.78755845	0.32303904
Tsyganenko [1995, 1996]	$-100 \le Dst \le 20$, $0.5 \le p \le 10$, $\lvert B_y\rvert \le 10$, $\lvert B_z\rvert \le 10$	0.78905312	0.70331884
Pfitzer et al. [1988]	$-100 \le Dst \le 20$, $300 \le v \le 500$, $5 \le n \le 50$	0.76007455	0.57903024
Olson and Pfitzer [1977]	None	0.68658362	0.42381700
Tsyganenko [1989]	$0 \le \mathrm{Kp} \le 9$	0.83894881	0.63889481
Tsyganenko [1987] long	$0 \le \mathrm{Kp} \le 9$	0.58069134	0.39857422
Tsyganenko [1987] short	$0 \le \mathrm{Kp} \le 9$	0.79734569	0.57341850
Fairfield and Mead [1975]	$0 \le \mathrm{Kp} \le 9$	0.76269466	0.51405170

[a]The input limit values are in units of nT for *Dst*, B_y, and B_z, nPa for *p*, m/s for *v*, and cm^{-3} for *n*.

characterized by quiet times and CIR stream interfaces (producing the infrequent geomagnetic storm), 2003 was marked by several severe CME-driven storms. These two storm mechanism give rise to very different storms (*Borovsky and Denton* [2006] enumerate 21 differences.)

[41] The most important difference for our study is storm intensity; CIR-driven storms rarely push *Kp* above 6, while CME-driven storms can push it up to 9 in extreme cases. The shape of the *Kp* profiles in Figures 2 and 3 reflect this: for 1996, the prediction efficiency drops off quickly near $Kp = 6$, while the 2003 plots indicate a more gradual drop off (at least for nonbasic models).

[42] Another difference between the 2 years is reflected in the MLT plots. The dawn and dusk dips in nonbasic models are more pronounced in 2003, when there were significant storms that would enhance contributions from the partial ring current and Birkeland currents. Interestingly, the basic models seem to have a somewhat less severe dayside dip in 2003 than 1996; this could be due to less variability in solar wind dynamic pressure or density for 2003 since there were fewer CIRs in 2003.

5.5. Impact of Model Inaccuracies on *L**

[43] One important question is: how much do model errors affect radiation belt studies? Radiation belt dynamics are only partially understood (see discussions by *Green and Kivelson* [2004], *Li and Temerin* [2001], and *Koskinen* [2005]). Adiabatic motions, those that conserve the three adiabatic invariants associate with the motion of a charged particle in a magnetic field [see *Wolf*, 1995], are well understood and must be identified and filtered out of the overall motion.

[44] One quantity of primary importance for this is the Roederer *L** parameter [*Roederer*, 1970], defined as

$$L^* = \frac{2\pi\mu_0}{\Phi R_E}, \tag{14}$$

where μ_0 is Earth's magnetic moment and Φ is a particle's third adiabatic invariant. Φ can be thought of as the flux enclosed by the drift shell of a particle on the given field line (i.e., at the given position). This parameter thus depends nonlocally upon the Earth's magnetic field. Since the Earth's field has not been measured except in particular small regions, *L** must be calculated from model fields.

[45] Calculation of this parameter can be computationally intensive. Table 5 lists *L** computation times for the models studied. It is evident that more sophisticated models take much longer to compute *L**. Thus, radiation belt researchers have incentive to use the fastest (i.e.,

Table 5. Computation Times for Total Field and *L**[a]

Model	Inputs	*B* Time (1 Week)	L^* Time (1 Day)
Tsyganenko et al. [2003]	*Dst*, *p*, B_y, B_z, *G*2, *G*3	0000:03	0231:07
Tsyganenko [2002a, 2002b]	*Dst*, *p*, B_y, B_z, *G*1, *G*2	0000:03	0355:35
Ostapenko and Maltsev [1997]	*Kp*, *Dst*, *p*, B_z	0000:01	0137:08
Tsyganenko [1995, 1996]	*Dst*, *p*, B_y, B_z	0000:01	0143:56
Pfitzer et al. [1988]	*Dst*, *v*, *n*	0000:01	0005:43
Olson and Pfitzer [1977]	None	0000:01	0003:50
Tsyganenko [1989]	*Kp*	0000:01	0004:10
Tsyganenko [1987] long	*Kp*	0000:01	0005:40
Tsyganenko [1987] short	*Kp*	0000:01	0004:31
Fairfield and Mead [1975]	*Kp*	0000:01	0003:04

[a]The computation times for *B* correspond to the time required to compute one week's worth of data with 1-min resolution. For L^*, the time corresponds to computing one day's worth of data.

Table 6. Typical Percent Differences in L^* and B for Magnetic Midnight, Dawn, Noon, and Dusk[a]

	$Kp < 4$		$Kp \geq 4$	
MLT	ΔB	ΔL^*	ΔB	ΔL^*
0000	5.928	6.318	6.508	4.851
0600	2.990	7.270	3.229	9.309
1200	3.738	3.407	3.757	5.835
1800	4.713	7.338	4.546	10.92

[a]Percent differences, denoted with Δ, are defined in equation (15). Notice ΔL^* is more sensitive at dawn and dusk and during disturbed periods.

simplest) model available. However, errors in the model must be considered when interpreting resulting data.

[46] An error in the model field will produce an error in the L^* value. Using the data here, a 2% difference in the model field produces as much as a 10% difference in L^*. This difference is defined as

$$\Delta L^* = \frac{|L^*_{T96} - L^*_{T02}|}{L^*_{T96}} \times 100, \quad (15)$$

with L^*_{T96} the value calculated with T96 and L^*_{T02} calculated with T02. A weak sinusoidal dependence on MLT value was found, with maxima close to dawn and dusk, and minima near noon and midnight. Table 6 gives typical values of the percent difference in L^* for dawn, dusk, noon and midnight.

5.6. Overstretching

[47] Overstretching refers to global overestimation of the distortion of Earth's internal field due to the solar

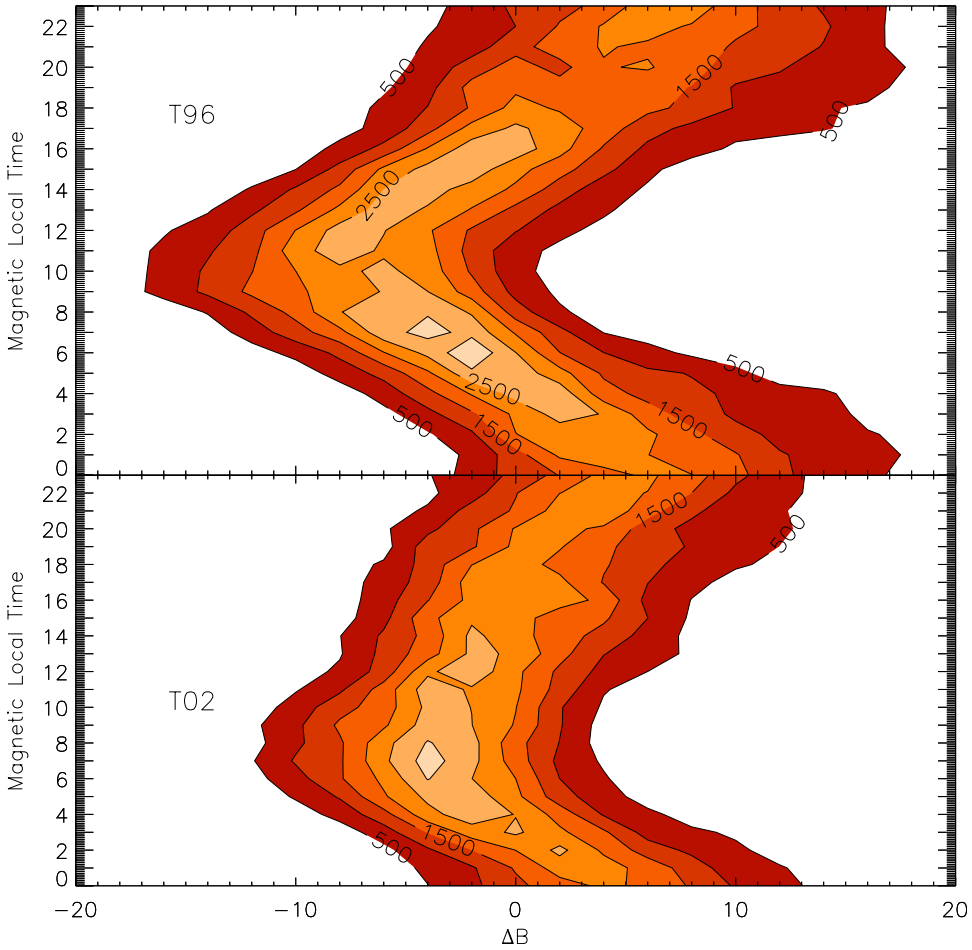

Figure 6. Contour plots of MLT-specific ΔB histograms. For a given MLT, the distribution of $\Delta B = \hat{B} - B_o$ is shown for (top) T96 and (bottom) T02. It is easy to see that T96 overestimates field strength on the dayside and underestimates it on the nightside more than T02. This is suggestive that the model overstretches the Earth's field.

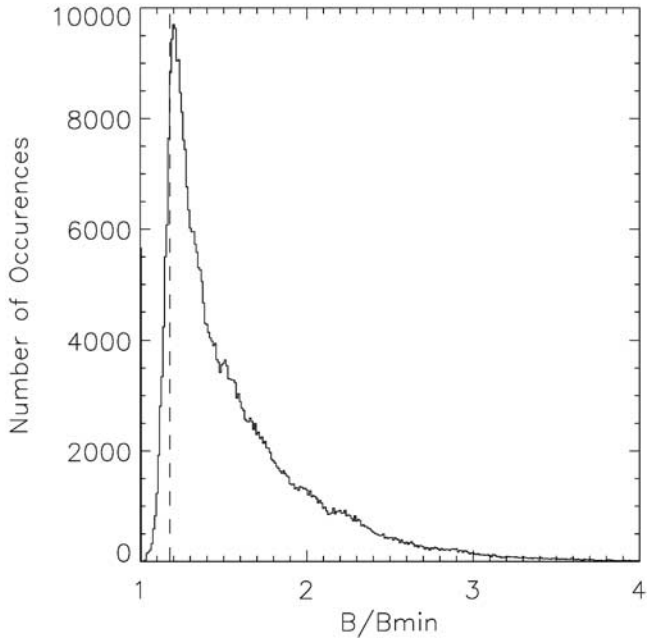

Figure 7. A histogram of the ratio B/B_{min}. B is the magnitude of the field measured at the GOES-8 position for the year 1996, corresponding to the data shown in Figure 6. B_{min} is the value of the field at the magnetic equator, according to the T96 model. The dashed line marks the value of B/B_{min} for the IGRF internal field with no external field and the idealized GOES-8 position (6.6 R_E, 0°N, 75°W).

wind. That is, the total magnetic field lines are too compressed on Earth's dayside and too stretched out on the nightside. TS87 and T89 have been previously shown to be overstretched in the midtail region [*Peredo et al.*, 1993]. There is evidence that T96 [*Huang et al.*, 2007; *Green and Kivelson*, 2004] is overstretched, and results here confirm that.

[48] We looked in detail at the error distribution for T96 as a function of magnetic local time. Figure 6 shows a contour plot of the error population in error value MLT space for two different models, T96 (top) and T02 (bottom). "Error" here is defined as $\Delta B = \hat{B}\text{-}B_o$, with $\hat{B}$ the model field and B_o the observed field. One can think of this as an overhead view of the histograms for each MLT stacked next to each other.

[49] The Figure 6 makes the overstretching readily apparent: for a given L value, on the dayside ($6 < MLT < 18$) a typical model field line corresponds to a weaker field than it should (the field lines are compressed), and on the nightside ($0 < MLT < 6$, $18 < MLT < 24$) a typical model field line corresponds to a stronger field than it should (the field lines are stretched out). Notice that both models are overstretched (this property of T02 is shown by *Stepanova et al.* [2007]), but T96 is more stretched. The global effect of overstretching is clearly seen in Figure 6, although the specific values near the midnight sector may be affected by a sensitive response to variations in the current sheet. This has the effect of widening the contours near midnight.

[50] To quantify the statistical importance of the current sheet, we made a histogram of the ratio of B/B_{min} (see Figure 7). The dashed line is the ratio for an idealized GOES position (6.6 R_E, 0°N, 75°W) with the IGRF internal field and no external field. The satellite is closer to the magnetic equator than this ideal scenario 10.05% of the time. This fact, coupled with the localized nature of the influence of the current sheet, confirms the overstretching is an effect of the model.

6. Conclusions

[51] We have shown how most of the models in the ONERA-DESP library perform for 2 years characterized by different phases in the solar cycle as well as different transient events. Not surprisingly, the newer models, particularly those that account for dawn-dusk asymmetry, perform best.

[52] Examining prediction efficiency as a function of MLT also led to some insight into the physical mechanisms that cause models to fail, and emphasized the importance of solar wind parameters and dawn-dusk asymmetrical contributions to the field. These contributions are significant, even during quiet periods. The exact nature of the dips seen near dawn and dusk is not known. Detailed study of the individual models and data sets employed by them could lead to a more thorough understanding of this.

[53] Prediction efficiency as a function of *Kp* suggests the range of utility for the different models. For $Kp < 4$, most models have prediction efficiencies greater than 0.5 (integrating over MLT), but for higher values of *Kp*, asymmetric models are significantly more robust than the other models studied.

[54] Comparison between the 2 years does not yield striking differences; for a given model, the performance during a quiet year with several CIRs is similar to the performance during a year marked by strong CME-driven storms. However, the only way to look in detail at CIR and CME differences is to do a storm-by-storm analysis; some work has been done in this area [*Huang et al.*, 2007].

[55] As shown in Section 5.5, the accuracy of a field model can significantly impact calculations in radiation belt studies. Thus, the choice of field model in these studies is very important, and should be taken into account when interpreting results. We conclude with a set of "rules" researchers can use to help determine which model might be best for their particular study:

[56] 1. These results indicate performance at geosynchronous orbit. If the region of study is significantly closer to Earth than this, the field is mostly internal in origin, so the choice of an external model shouldn't affect things greatly. If the region of study is significantly farther away (e.g., in the tail), these results should not be used exclusively. Other studies that focus on the region, such as *Peredo et al.* [1993], should be consulted as well if available.

[57] 2. Basic models perform very poorly on the dayside. If the region under examination intersects the dayside magnetosphere, these models should not be used, even during quiet periods.

[58] 3. T96 is a very popular model. It is fast and performs better than the basic models. However, it is likely significantly overstretched. This must be considered when using L^* values computed from T96.

[59] 4. T02 performs better than T96, even accounting for the input bias; in fact, "T96 should be considered valid during quiet times only," (S. Bourdarie, Input range in the T02 model, personal communication, 2008). T02 should be used in place of T96 for $Kp < 6$ where possible. TSK03 is a much more suitable choice during storm time conditions ($Kp > 6$), since it can handle extreme solar wind inputs.

[60] 5. If the region of study is near dawn or dusk, extra caution must be used when interpreting results, as all models tend to perform most poorly there, and L^* values are particularly sensitive to model differences.

[61] 6. The geomagnetic conditions during a selected period of study may determine the use of a particular model, because of the restrictions on model input. However, it should be remembered that the loss in prediction efficiency is particularly strong during these times, and the overall prediction efficiency for a model may not accurately represent it's behavior during extreme times.

[62] **Acknowledgments.** The authors would like to thank T. P. O'Brien, S. Elkington, S. Bourdarie, X. Li, J. C. Green, D. Turner, E. J. Rigler, T. Onsager, and H. Singer for helpful discussions and insightful comments. This research was undertaken with the support of NASA grants NNG04GN11G and NNG05GK04G.

References

Alexeev, I. I., E. S. Belenkaya, and C. R. Clauer Jr. (2000), A model of region 1 field-aligned currents dependent on ionospheric conductivity and solar wind parameters, *J. Geophys. Res.*, *105*(A9), 21,119–21,127.

Baker, D. N., S. G. Kanekal, X. Li, S. P. Monk, J. Goldstein, and J. L. Burch (2004), An extreme distortion of the Van Allen belt arising from the 'Hallowe'en' solar storm in 2003, *Nat.*, *432*, 878–881.

Baker, D. N., S. R. Elkington, X. Li, and M. J. Wiltberger (2005), Particle acceleration in the inner magnetosphere, in *The Inner Magnetosphere: Physics and Modeling*, *Geophys. Monogr. Ser.*, vol. *155*, edited by T. I. Pulkkinen, N. A. Tsyganenko, and R. H. W. Friedel, pp. 73–85, AGU, Washington, D.C.

Borovsky, J. E., and M. H. Denton (2006), Differences between CME-driven storms and CIR-driven storms, *J. Geophys. Res.*, *111*, A07S08, doi:10.1029/2005JA011447.

Chen, Y., R. H. W. Friedel, G. D. Reeves, T. E. Clayton, and R. Christensen (2007), Multisatellite determination of the relativistic electron phase space density at geosynchronous orbit: An integrated investigation during geomagnetic storm times, *J. Geophys. Res.*, *112*, A11214, doi:10.1029/2007JA012314.

Fairfield, D. H., and G. D. Mead (1975), Magnetospheric mapping with a quantitative geomagnetic field model, *J. Geophys. Res.*, *80*, 535–542.

Green, J. C., and M. G. Kivelson (2004), Relativistic electrons in the outer radiation belt: Differentiating between acceleration mechanisms, *J. Geophys. Res.*, *109*, A03213, doi:10.1029/2003JA010153.

Huang, C.-L., H. E. Spence, H. J. Singer, and N. A. Tsyganenko (2007), A quantitative assessment of empirical magnetic field models at geosynchronous orbit during magnetic storms, *J. Geophys. Res.*, *113*, A04208, doi:10.1029/2007JA012623.

Kamide, Y., et al. (1998), Current understanding of magnetic storms: Storm-substorm relationships, *J. Geophys. Res.*, *103*(A8), 17,705–17,728.

Koskinen, H. E. J. (2005), Energetic particle losses from the inner magnetosphere, in *The Inner Magnetosphere: Physics and Modeling*, *Geophys. Monogr. Ser.*, vol. *155*, edited by T. I. Pulkkinen, N. A. Tsyganenko, and R. H. W. Friedel, pp. 23–31, AGU, Washington, D.C.

Li, X., and M. A. Temerin (2001), The electron radiation belt, *Space Science Rev.*, *95*(1–2), 569–580, doi:10.1023/A:1005221108016.

Olson, W. P., and K. A. Pfitzer (1977), Magnetospheric magnetic field modeling, *Annu. Sci. Rep. F44620-75-C-0033*, Air Force Off. of Sci. Res., Arlington, Va.

Ostapenko, A. A., and Y. P. Maltsev (1997), Relation of the magnetic field in the magnetosphere to the geomagnetic and solar wind activity, *J. Geophys. Res.*, *102*(A8), 17,467–17,473.

Peredo, M., D. P. Stern, and N. A. Tsyganenko (1993), Are existing magnetospheric models excessively stretched?, *J. Geophys. Res.*, *93*(A9), 15,343–15,354.

Pfitzer, K. A., W. P. Olson, and T. Mogstad (1988), A time dependent source driven magnetospheric magnetic field model, *Eos Trans. AGU*, *69*, 426.

Pulkkinen, T. I., and N. A. Tsyganenko (1996), Testing the accuracy of magnetospheric model field line mapping, *J. Geophys. Res.*, *101*(A12), 27,431–27,442.

Reeves, G. D., L. A. Weiss, M. F. Thomsen, and D. J. McComas (1996), A quantitative test of different magnetic field models using conjunctions between DMSP and geosynchronous orbit, in *Radiation Belts: Models and Standards*, *Geophys. Monogr. Ser.*, vol. *97*, edited by J. F. Lemaire et al., pp. 167–172, AGU, Washington, D.C.

Roederer, J. G. (1970), *Dynamics of Geomagnetically Trapped Radiation*, Cambridge Univ. Press, New York.

Spence, H. E., M. G. Kivelson, and R. J. Walker (1987), Static magnetic field models consistent with nearly isotropic plasma pressure, *Geophys. Res. Lett.*, *14*(8), 872–875.

Stepanova, M., E. E. Antonova, and J. M. Bosqued (2007), Radial distribution of the inner magnetosphere plasma pressure using low-altitude satellite data during geomagnetic storm: The March 1–8, 1982 event, *JAdv. Space Res.*, *41*, 1658–1665, doi:10.1016/j.asr.2007.06.002.

Stern, D. P. (1994), The art of mapping the magnetosphere, *J. Geophys. Res.*, *99*(A9), 17,169–17,198.

Tascione, T. F. (1994), Introduction to the Space Environment, 2nd ed., chap. 4, pp. 50–51, Krieger, Melbourne, Fla.

Thomsen, M. F., D. J. McComas, G. D. Reeves, and L. A. Weiss (1996), An observational test of the Tsyganenko (T89a) model of the magnetospheric field, *J. Geophys. Res.*, *101*(A11), 24,827–24,836.

Tsyganenko, N. A. (1987), Global quantitative models of the geomagnetic field in the cislunar magnetosphere for different disturbance levels, *Planet. Space Sci.*, *35*, 1347–1358.

Tsyganenko, N. A. (1989), A magnetospheric magnetic field model with a warped tail current sheet, *Planet. Space Sci.*, *37*, 5–20.

Tsyganenko, N. A. (1995), Modeling the Earth's magnetospheric magnetic field confined within a realistic magnetopause, *J. Geophys. Res.*, *100*(A4), 5599–5612.

Tsyganenko, N. A. (1996), Effects of the solar wind conditions on the global magnetospheric configuration as deduced from data-based field models, in *Proceedings of the 3rd International Conference on Substorms (ICS-3)*, pp. 181–185, Eur. Space Agency, Versailles, France.

Tsyganenko, N. A. (2002a), A model of the near magnetosphere with a dawn-dusk asymmetry: 1. Mathematical structure, *J. Geophys. Res.*, *107*(A8), 1179, doi:10.1029/2001JA000219.

Tsyganenko, N. A. (2002b), A model of the near magnetosphere with a dawn-dusk asymmetry: 2. Parameterization and fitting to observations, *J. Geophys. Res.*, *107*(A8), 1176, doi:10.1029/2001JA000220.

Tsyganenko, N. A. (2005), Modeling the dynamics of the inner magnetosphere during strong geomagnetic storms, *J. Geophys. Res.*, *110*, A03208, doi:10.1029/2004JA010798.

Tsyganenko, N. A., and D. P. Stern (1996), Modeling the global magnetic field of the large-scale Birkeland current systems, *J. Geophys. Res.*, *101*, 27,187–27,198.

Tsyganenko, N. A., H. J. Singer, and J. C. Kasper (2003), Storm-time distortion of the inner magnetosphere: How severe can it get?, *J. Geophys. Res.*, *108*(A5), 1209, doi:10.1029/2002JA009808.

Vassiliadis, D. (2007), Forecasting space weather, in *Space Weather: Physics and Effects*, edited by V. Bothmer and I. A. Daglis, chap. 14, pp. 419–420, Springer, New York.

Walker, R. J. (1976), An evaluation of recent quantitative magnetospheric magnetic field models, *Rev. Geophys.*, *14*(3), 411–427.

Wolf, R. A. (1995), Magnetospheric configuration, in *Introduction to Space Physics*, edited by M. G. Kivelson and C. T. Russell, chap.10, pp. 288–325, Cambridge Univ. Press, New York.

D. N. Baker, M. Gehmeyr, and J. P. McCollough, Laboratory for Atmospheric and Space Physics, University of Colorado, 1234 Innovation Drive, Boulder, CO 80303, USA. (james.mccollough@colorado.edu)

J. L. Gannon, Space Weather Prediction Center, National Oceanic and Atmospheric Administration, 325 Broadway Street, Boulder, CO 80305, USA.